Received Date : 06-Oct-2015
Revised Date : 16-Jun-2016
Accepted Date : 18-Jun-2016
Article type : Article

Contributing editor: Vikram Jayaram
Corresponding Author Email ID: wingbrad@umich.edu

Microstress in Reaction Bonded SiC from Crystallization Expansion of Silicon

Authors: Bradley L. Wing, Francis Esmonde-White, John W. Halloran

Abstract

Microstress in reaction-bonded silicon carbide (RBSiC) has been measured using piezo-Raman spectroscopy. Compressive microstresses as high as 2 GPa exist in the silicon phase and tensile microstresses as high as 2.3 GPa exist in the SiC phase of RBSiC. This is much larger than expected for thermoelastic microstress from coefficient of thermal expansion mismatch would provide. Instead the

This is the author manuscript accepted for publication and has undergone full peer review but has not been through the copyediting, typesetting, pagination and proofreading process, which may lead to differences between this version and the Version of Record.
Please cite this article as doi: 10.1111/jace.14398

This article is protected by copyright. All rights reserved

Author Manuscript

microstresses arise from the crystallization of liquid silicon. During the reaction bonding process, not all of the silicon reacts to form SiC and there is liquid free silicon. The phase transformation of the free silicon from liquid to solid has a large volume expansion, which results in large residual microstress within the silicon and SiC phases of RBSiC.

1 Introduction

Silicon carbide is a very useful material for a number of applications due to its high temperature capabilities, high thermal conductivity, and low density. There are many ways of manufacturing SiC including powder sintering, chemical vapor deposition (CVD), pyrolysis of silicon containing polymer preforms, as well as other techniques[1]. Reaction bonding is a prominent technique[2-4], where a preform is converted to SiC by the reaction of liquid silicon with a source of carbon, and is often conducted by melt-infiltration (MI) of liquid silicon into a carbon preform[5,6]. By melt-infiltration, fully dense RBSiC can be made to net shape at relatively low temperatures, with relatively fast manufacturing[7].

In the MI process, silicon carbide is formed by the reaction of liquid silicon alloy with a carbon source to form a rigid SiC network. Typically, a significant fraction of the silicon is left unreacted, so that the RBSiC is a two-phase mixture of SiC and free silicon [5]. While RBSiC is a well-known material and process, the existence of large residual microstress on the scale of the grain size is a little-recognized attribute. In this paper, we present measurements of the compressive microstress in the free silicon phase and tensile microstresses in the SiC phase. We propose that these microstresses arise from the crystallization of the free silicon liquid during cooling.

Liquid silicon is a random dense packed liquid, but crystalline silicon is a tetrahedral solid with a significantly lower density. The density difference between the liquid and crystal causes the silicon volume fraction to expand by about 10.8% upon solidification, which creates a crystallization expansion strain (CES). The phenomenon of crystallization expansion of the free silicon has been noted by

Author Manuscript

This article is protected by copyright. All rights reserved

Hillig[8], but he makes no reference to its role in the resulting microstresses. The SiC network is rigid, and so silicon crystallization must either expel some of the liquid silicon, or SiC network must constrain the silicon phase. Preventing the silicon expansion causes a residual microstress state. The constrained silicon phase must experience a compressive residual microstress while the constraining SiC phase must experience a tensile residual microstress. This paper addresses the measurement of these microstresses and relates it to approximate stress values arising from the constraint of crystallization expansion strain.

2 Materials and Experimental Methods

2.1 Materials and Microstructural Characterization

We examine two commercial grades of reaction-bonded silicon carbide (RBSiC) with two markedly different volumes fractions of free silicon. The lower-silicon RBSiC material is SC-2 is received from Coors Tek in 2014, and the higher-silicon RBSiC is KXO1 and was manufactured by Carborundum around 1986 and was provided by Sheldon Wiederhorn from samples of a material used in a previous study of creep[9]. The volume fraction of the free silicon phase was determined by examining more than 80 fields of view of polished surfaces, imaged optically at 200x using a Nikon Eclipse ME600L microscope. The silicon phase was isolated with a threshold function and its area fraction determined using Matlab.

The free silicon fraction was independently determined with quantitative X-ray diffraction (XRD) using the internal standards method. An internal standard was created using known volumes of silicon powder and the RBSiC material, which has an unknown amount of free silicon. The integrated intensity ratios depend on the total amount of silicon. This is the known amount of silicon powder as well as the unknown amount of native silicon in the RBSiC material. Standards consisted of 0, 10, 20, 30, and 40 vol% silicon with the remaining volume made up of RBSiC. The integrated intensity of the (111), (220), and (311) peaks of silicon compared with the (101), (102), (103), (104), and (110) α-SiC peaks. The diffraction patterns were

This article is protected by copyright. All rights reserved

Author Manuscript

collected with a Rigaku Miniflex over the range from 10-65° using a scan rate of 1°/min with a step size of 0.02°.

2.2 Raman Spectroscopy Method

We measured the residual microstress state in the silicon phase and SiC phase using Raman microspectroscopy, which is a common technique used to determine the residual microstress state in a material[10–12]. Raman spectroscopy is a measurement of inelastic light scattering arising from the polarizability of the vibrational modes. Molecular species have Raman emission bands with characteristic frequencies. As stress is applied, the position of the Raman peaks will shift. Shifts in Raman band can be used to infer the stress on the material with very high spatial resolution.

The difference between the peak position of the unstressed state and the microstress state is measured as a wavenumber shift, $\Delta\omega$[13]. This shift can be used to calculate the current microstress state based on the equation

$$\Delta\omega = R\sigma \quad [1]$$

where R is the coefficient relating the Raman shift to the stress, and σ is the effective stress experienced by the corresponding phase.

Silicon has a well-defined, single Raman peak at 520 cm^{-1} and a Raman coefficient of 1.88 ± 0.05 cm^{-1}/GPa has been measured by Anastakakis et al[14]. The Raman spectrum of SiC is more complicated, having a triplet transverse optic (TO) peak and a broad longitudinal optic (LO) peak. DiGregorio and Furtak have analyzed the TO peak of polycrystalline SiC[15], and fit the full triplet of the TO as a single peak, with an unstressed state of 797 cm^{-1}. They determined a Raman coefficient for the TO peak in polycrystalline SiC to be 3.53 ± 0.21 cm^{-1}/GPa. This will serve as the Raman coefficient for both α and β-SiC[15,16]

For the microstress magnitudes reported here, all silicon stresses have been calculated using the Raman coefficient defined by Anastkakis et al., and all SiC stresses will be based on the TO curve and the Raman coefficient defined by DiGregorio and Furtak.

This article is protected by copyright. All rights reserved

Author Manuscript

A custom Raman microspectroscopy system was used in this work[17,18]. A fiber optic coupled 532 nm green laser (Innovative Photonics) was collimated and reflected off a dichroic filter (SEMROCK). The dichroic filter brought the laser onto the same axis as the Raman scattering collection path. The laser was directed into a Nikon Eclipse ME600L microscope using a custom-built turning mirror turret. The laser passed through the microscope optics in an epi-illumination geometry, and focused into a spot size of 20 μm at the sample surface providing energy for Raman scattering.

The Raman scattered photons from the sample are collected back through the microscope optics, passing through the dichroic as the Raman emission wavelength is longer than the source laser light. The dichroic acts to first bring the laser light onto the same path as the collection beam, and also to filter out 532 nm laser light. A notch filter (SEMROCK) was placed behind the dichroic to provide additional laser rejection prior to a second collimating objective which fiber-coupled the collection beam. By removing residual laser excitation power, the notch filter eliminates interfering Raman scattering from SiO_2 in the fiber optics. The collection fiber optic then delivered the collected Raman signal into a HoloSpec VPT spectrograph (Kaiser Optical Systems, Inc.). In the spectrograph the Raman scattered light is dispersed by the grating such that different wavelengths of light are measured at different physical locations across the imaging detector (charged coupling device, CCD). A Newton EM CCD (ANDOR) was used to measure the Raman scattered light and transmit the recorded signal to a computer for analysis in Matlab (MathWorks).

To confirm that the Raman band shift could be plausibly related to stress, we performed a limited number of experiments using a flexural fixture to apply a known applied stress to the specimen[19]. The observed shifts were consistent with the R coefficients we use from the literature[14,15].

Author Manuscript

This article is protected by copyright. All rights reserved

3 Results: Microstress from Raman Measurements

3.1 Microstructure and Free Silicon

Figure 1 illustrates the microstructure as optical images of polished sections for each grade. The images show two interpenetrating networks consisting of silicon (light grey) and SiC (dark grey). In these images, we can see the extent of the unreacted free silicon. The characteristic size of the SiC phase, inferred from linear intercept measurements, varies from 1.9-4.8 μm in the low-Si material, with the free silicon phase having a characteristic size of 0.6-4.6 μm. The SiC phase is somewhat smaller in the high-Si material, 1.3-2.8 μm, with the free silicon region in the range 0.8-1.8 μm.

Image analysis determined the volume fraction of free silicon to be 20 ± 4 vol% for the low-Si material and 40 ± 6 vol% for high-Si material. These values represent the mean volume fraction average of 80 fields of view with the variation representing the range of repeated analyses.

For the XRD analysis, the method of internal standards was used. In Figure 2 we show the ratio of the integrated intensities for the three silicon peaks over the total integrated intensity (silicon and SiC), plotted against the added weight percent of silicon powder. The overall volume of silicon was determined using the form:

$$\frac{I_{Si}}{I_{Si}+I_{SiC}} = m\left[x + (1-x) f_{Si}^{RBSiC}\right] \qquad [2]$$

where I is the integrated intensity of the respective phase, x is the mass of pure silicon added to the powder, f_{Si}^{RBSiC} is the volume fraction of silicon phase in the RBSiC material, and m is a constant determined experimentally. The amount of silicon in the RBSiC material is constant. Using the relationship in Eq [2], we were able to determine the unknown weight percent of silicon in the RBSiC material. Using the density of silicon and SiC, we were able to convert the weight percent of the silicon determined using XRD to a volume percentage. XRD shows that the silicon content in the high-Si RBSiC is 42 ± 1% and the constant m is 1.048. Note that this value is higher than the 33 vol% of silicon that was reported in Wiederhorn et al. However, since the image analysis and quantitative XRD analysis were performed

This article is protected by copyright. All rights reserved

Author Manuscript

separately and are in agreement, we will use the value of 42 ± 1 volume percent. For the low-Si material, the free silicon volume fraction was determined to be 24 ± 1%. Both of these silicon contents determined through powder XRD are in very good agreement with values obtained by image analysis.

3.2 Microstress from Raman Measurements

Raman spectra were recorded at 20 different positions on each sample. Using a spot size of 20 μm, we were able to include more than 10 SiC grains and the surrounding free silicon within each spot. Four different samples of the high and low silicon materials were examined. Figure 3 shows typical spectra for 4 locations in a sample with high-Si content. The positions of the spots are illustrated in the microstructure in Figures 3a – 3d. The complete spectrum, including the Si peak near 520 cm^{-1} and the SiC peak near 797 cm^{-1}, are in Figure 3e for the four locations. Figure 3f shows in detail the region of the silicon peak. Notice that the spectra from the four locations overlap. The unstressed silicon peak location is shown as a line at 520 cm^{-1}. The observed peaks are centered around 523 cm^{-1}, indicating a red-shift which we interpret as arising from a compressive microstress in the free silicon phase. For the silicon carbide phase Figure 3g shows the four observed spectra for the TO SiC peak with the unstressed peak location shown at 797 cm^{-1}. These have different intensities, but all are centered around 787-789 cm^{-1}. The blue shift from the unstressed peak indicates the presence of tensile stresses in the SiC phase.

Figure 4 has similar information from 4 typical locations for the low-Si material, showing the locations of the probed region (Figure 4a – 4d), the four spectra (Figure 4f) and details of the Raman peaks from the silicon phase (Figure 4f) and Raman peaks from the SiC phase (Figure 4g).

Table I lists the measured peak locations for the 4 example positions for both samples, and the residual microstress calculated using a piezoraman coefficient of 1.88 ± 0.05 cm^{-1}/GPa for the 520 Si peak and 3.53 ± 0.21 cm^{-1}/GPa for the TO peak in polycrystalline SiC. For these examples, the silicon phase is shown to have a compressive residual microstress of around 1.74-1.88 GPa, while the SiC phase has a tensile residual microstress of 2.13-2.37 GPa in high-Si material and 1.77-2.08 GPa

This article is protected by copyright. All rights reserved

of compression in silicon and 2.10-2.43 GPa of tension in SiC in the low-Si material. These values correspond to the spectra in Figure 3 and Figure 4.

Table II presents all the data for both grades of RBSiC, for 20 locations in each of 4 specimens of each material. Each value is the result of 20 spectra taken at different points on the polished sample. The variation reported in Table II is the result of the variation from position to position and the error in the Raman coefficient from the literature. The two types of variation were determined for each data set, and then added together to determine the final error reported. The results of Eq. [1] from each spectrum are averaged together for the reported residual microstress measurement. The measured stresses are consistent from sample to sample. The location-to-location variation is taken into account within the error calculation. The error reported also includes the peak fitting error and the reported Raman coefficient error.

4 Discussion

The inferred stress values found in both of the RBSiC materials are very large. These large microstresses exist in commercially available RBSiC as well as RBSiC produced in a lab more than 25 years prior to this study. For the compressive microstress measured in the silicon, the low-Si material (mean value of 1.92 ± .11 GPa) showed a slightly higher magnitude than that of the measured compressive microstress in the silicon phase of the high-Si material (mean value of 1.76 ± .15 GPa). Conversely, the low-Si material, has a lower residual tensile microstress in the SiC phase (mean value of 2.12 ± .22 GPa) than that of the SiC phase in the high-Si material (mean value of 2.28 ± .10 GPa).

These stresses are very large, and have not been reported in previous studies. Two potential sources for these large stresses were investigated: (1) as a result of a coefficient of thermal expansion mismatch (thermoelastic stresses) and (2) as a result of the crystallization expansion of silicon during processing. We will evaluate the magnitude of these two sources of stress and determine which contributes most to the measured microstresses or if there is equal contribution.

This article is protected by copyright. All rights reserved

Author Manuscript

4.1 Thermoelastic Stresses

Microstresses in two-phase materials are conventionally understood in terms of the thermoelastic effects that arise upon cooling due to the difference in thermal expansion between the two phases. As the thermoelastic coefficient (TEC) of silicon is smaller than the TEC of SiC, one would anticipate that, upon cooling the silicon would endure a compressive residual microstress and the SiC would have a corresponding tensile residual microstress. Thermoelastic stresses are in the correct sense (compressive in silicon, tensile in SiC), but are the magnitudes of the values measured by Raman consistent with thermoelastic stresses? We examined the microstress induced from a coefficient of thermal expansion (CTE) mismatch. A CTE mismatch calculation was done for silicon and SiC using the classical model developed for thermoelastic microstress in two-phase composites by Kingery[20], which is based on the work of Turner[21]. This model ignores relaxation and has a simple geometry, but provides an estimate of the anticipated magnitude of the thermoelectric residual microstresses.

Both silicon and SiC have CTEs that vary with temperature. CTE curves from the literature were used[22,23]:

$$\alpha_{SiC} = 3.19 * 10^{-6} + 3.60 * 10^{-9}T - 1.68 * 10^{-12}T^2 \quad [^{\circ}\mathrm{C}^{-1}] \qquad [3]$$

$$\alpha_{Si} = \begin{pmatrix} 3.725\{1 - \exp[-5.88 * 10^{-3}(T - 397)]\} \\ +5.548 * 10^{-3}(T - 273) \end{pmatrix} * 10^{-3}\ [^{\circ}\mathrm{C}^{-1}] \qquad [4]$$

where α is the coefficient of thermal expansion and T is the temperature. The thermoelastic Kingery-Turner solution follows the form:

$$\sigma_{Si} = (\alpha_r - \alpha_{Si})\Delta T K_{Si} \qquad [5]$$

for the silicon phase, and for the SiC phase,

$$\sigma_{SiC} = (\alpha_r - \alpha_{SiC})\Delta T K_{SiC} \qquad [6]$$

where σ is the thermoelectric microstress, K is the bulk modulus for that phase, α is the coefficient of thermal expansion, and ΔT is the difference between the initial and final temperature. The subscript r denotes the CTE of the two phase mixture and can be expressed in terms of the volume fraction V_{Si} and V_{SiC}:

$$\alpha_r = \frac{\alpha_{\mathrm{Si}}K_{\mathrm{Si}}V_{\mathrm{Si}} + \alpha_{\mathrm{SiC}}K_{\mathrm{SiC}}V_{\mathrm{SiC}}}{K_{\mathrm{Si}}V_{\mathrm{Si}} + K_{\mathrm{SiC}}V_{\mathrm{SiC}}} \qquad [7]$$

This article is protected by copyright. All rights reserved

Author Manuscript

We can then solve α_r using the CTEs in Eq. 3 and Eq. 4 as well as the relevant values found in Table III[24,25]. This uses room temperature bulk modulus for silicon and SiC, which is adequate within the degree of approximation of the Kingery-Turner model. We will keep the α_r term for simplicity purposes. We then integrated Eq. 5 from the melting temperature of silicon (1410°C) to room temperature (25°C):

$$\sigma_i = K_i \int_{1410}^{25} (\alpha_r - \alpha_i) dT \quad [8]$$

Results of Eq. 7 can be seen in Table IV for both phases in each material. The thermoelastic microstresses calculated from the CTE mismatch are between 0.085-0.10 GPa compression for the silicon phase and 0.031-0.061 GPa tension in the SiC phase. These thermoelastic values more than an order of magnitude lower than the measured residual microstress. Therefore, we suspect that the microstress measured using Raman spectroscopy do not arise primarily from thermal expansion mismatch.

4.2 Stress from Crystallization Expansion of Silicon

Now consider the crystallization expansion of silicon. During the MI process, there is residual silicon, which expands when it solidifies. The expansion of the silicon places the solid silicon in a state of compression, as the silicon expansion is constrained by the surrounding rigid network of silicon carbide. The silicon carbide network is then in a state of tension to balance the stress in the silicon. This phase transformation produces the correct sense of the residual stresses observed by Raman spectroscopy.

To estimate the magnitude of the stress developed by the crystallization expansion of the silicon, we can consider the unrelaxed crystallization strain. The density of solid silicon at 1410°C is 2.32 g/cm^3 and the density of liquid silicon at 1410°C is 2.57 g/cm^3. Therefore, when the silicon transforms from liquid to solid, there is a volumetric expansion in the silicon phase of about 11%. This results in a linear crystallization expansion strain, ε_{CES} = 0.036.

To evaluate the stress developed by this strain, we will modify the classical Kingery-Turner thermoelastic model so that it can be used with crystallization expansion strain rather than thermal expansion mismatch strain. Since the $\alpha\Delta T$

This article is protected by copyright. All rights reserved

Author Manuscript

portion of the relationship represents a strain, we can substitute the strain for the crystallization expansion strain (CES) of the silicon from the phase transformation, and simply use that for a modified Kingery-Turner model.

To estimate the strain in the Si-SiC two phase mixture, ε_{comp}, created by the crystallization in the silicon phase, we make use of Eq. 5 – 7. In place of the term $\alpha_r\Delta T$, we use ε_{comp} to represent the composite strain. The silicon phase transforms, and in place of $\alpha_{Si}\Delta T$, we use ε_{CES}. There is no phase transformation for the SiC in the temperature range of interest. So, the expansion strain of the Si-SiC mixture associated with crystallization of the liquid silicon is:

$$\varepsilon_{comp} = \frac{\varepsilon_{CES} K_{Si} V_{Si}}{K_{Si} V_{Si} + K_{SiC} V_{SiC}} \quad [9]$$

We can then use this in an expression like Eq. 5, and we expect for the microstress in the SiC phase to be:

$$\sigma_{SiC} = \varepsilon_{comp} K_{SiC} \quad [10]$$

and the microstress in the silicon phase to be:

$$\sigma_{Si} = K_{Si}\left(\varepsilon_{comp} - \varepsilon_{CES}\right) \quad [11]$$

The magnitude of the microstresses from crystallization expansion strain from Eq. 11 are presented in Table V. We anticipate about 3 GPa of compressive stress in the silicon phase for the low-Si sample. However, from the measured Raman shifts, we observe a compressive stress in the range of 1.9 GPa for the silicon in this sample. For the sample with the higher silicon, we expect 2.7 GPa of compressive stress based on Eq. 11, but we observe 1.8 GPa due to the measured peak shift in the Raman signal. This simple model is in the right order of magnitude, but overestimates the compressive stress in the silicon phase by about 50% for both samples in this study.

The tensile stress in the SiC phase is underestimated by the modified Kingery-Turner expression in Eq. 10. In the low silicon specimen, we anticipate about 1 GPa of tensile stress in the SiC phase, but the Raman measurements indicate about 2.15 GPa of tensile stress. For the high silicon specimen, the model anticipates about 2.7 GPa compared to the measured 2.28 GPa.

This article is protected by copyright. All rights reserved

Author Manuscript

5 Conclusion

There are intense microstress in the constituent phases of reaction bonded silicon carbide SiC and free silicon that have previously not been discussed in the literature. The free silicon phase carries compressive stress on the order of 1.7-2 GPa, while the silicon carbide phase carries a tensile stress in the range of 2.1-2.4 GPa. The measured microstresses in the silicon phase and the SiC phase are much larger than what a CTE mismatch can account. We have shown that the large residual microstress state in MI-RBSiC can be plausibly attributed to the volumetric changes during crystallization of the unreacted silicon. We have modified the Kingery-Turner thermoelastic stress model to determine the stress in the silicon and SiC phases anticipated from crystallization expansion strain. This model shows probably relationship between the measured residual stress state in the silicon and SiC phases of RBSiC and the crystallization expansion of silicon in the two-phase mixture.

Acknowledgement

The authors thank Professor Michael Morris for guidance and use of the Raman microscopy equipment in his laboratory. We have appreciated working with him immensely. We thank Prof. Nina Orlovskaya and Richard Stadelmann at the University of Central Florida for access to their flexural test coupled with Raman spectroscopy. This research was funded by GE Aviation, under a University Strategic Alliance grant.

References:

1. L. L. Snead, T. Nozawa, Y. Katoh, T. S. Byun, S. Kondo, and D. A. "Petti, Handbook of SiC Properties for Fuel Performance Modeling," *J Nucl Mater.*, **371**, 329-377 (2007)

2. K. Luthra, R. Singh, M. K. Brun, "Toughened Silcomp Composites - Process and Preliminary Properties", *Am Ceram Soc Bull.*, **72**, 79 (1993)

This article is protected by copyright. All rights reserved

Author Manuscript

3. P. Popper, ed. *Special Ceramics*. London: British Ceramic Research Association; (1960)

4. Y. M. Chiang, R. P. Messner, C. D. Terwilliger, and D. R. Behrendt, "Reaction-Formed Silicon Carbide", *Materials Science and Engineering A*., **A144**, 63-74 (1991)

5. H. Zhou and R. N. Singh, "Processing and Microstructural Characterization of Melt-Infiltrated Si/SiC Composites". *J Materials Synthesis and Processing*, **4**, 125-134 (1997)

6. M. Singh and D. R. Behrendt. "Studies on the Reactive Melt Infiltration of Silicon and Silicon-Molybdenum Alloys in Porous Carbon". *NASA TM-105860,* (1992)

7. G.R. Sawyer and T.F. Page, "Microstructural Characterization of "REFEL" (Reaction-Bonded) Silicon Carbides", *J Materials Science*., **13**, 885-904 (1978)

8. W.B. Hillig. "Melt Infiltration Process for Making Ceramic Matrix Composites In:. *Fiber Reinforced Ceramic Composites*. K. S. Mazdiyasni, editor, Park Ridge, NJ: Noyes Publications; 261-277 (1990)

9. S. M. Wiederhorn, B. J. Hockey, and J. D. French, "Mechanisms of Deformation of Silicon Nitride and Silicon Carbide at High Temperatures", *J European Ceram Soc*., **19**, 2273-2284 (1999)

10. P. Colomban, G. Gouadec, J.Mathez, J. Tschiember and P. Peres, "Raman Stress Measurement in Opaque Industrial C/Epoxy Composites Submitted to Tensile Strain". *Composite. Part A*, **37** [4] 646-651 (2006)

11. J. Watts, G. Hilmas, W.G. Fahrenholtz, D. Brown and B. Clausen, "Stress Measurements in ZrB2-SiC using Raman Spectroscopy and Neutron Diffraction". *J European Ceramic Soc*., **30**, 2165-2171 (2010)

12. N. Ferralis, "Probing Mechanical Properties of Graphene with Raman Spectroscopy", *Journal of Materials Science*., **45** [19] 5135-49 (2010)

13. D. Sciti, S. Guicciardi, G. Celotti, M. Deluca, and G. Pezzotti, "Residual Stress Investigation in SiC/MoSi2 Composites". *Advanced Engineering Materials*, **9**, 393-399 (2007)

Author Manuscript

This article is protected by copyright. All rights reserved

14. E. Anastassakis, A. Cantarero and M. Cardona, "Piezo-Raman measurements and anharmonic parameters in silicon and diamond" *Phys Rev B.*, **41**, 7529-7535 (1990)

15. J. F. DiGregorio and T. E. Furtak, "Analysis of Residual Stress in 6H-SiC Particles within Al2O3/SiC Composites through Raman Spectroscopy". *J American Ceram Soc.*, **75**, 1854-1857 (1992)

16. J. F. DiGregorio, T. E. Furtak and J. J. Petrovic, "A Technique for Measuring Residual Stress in SiC Whiskers within an Alumina Matrix through Raman Spectroscopy", *J Applied Physics.*,**71**, 3524-3531 (1992)

17. K. A. Esmonde-White, F. W. L. Esmonde-White, M. D. Morris. B. J. Roessler, "Fiber-optic Raman Spectroscopy of Joint Tissues". *Analyst.*,**136**, 1675-1685 (2011)

18. F. W. L. Esmonde-White and M. D. Morris. "Raman Imaging and Raman Mapping." pp. 97-110 in: *Emerging Raman Applications and Techniques in Biomedical And Pharmaceutical Fields*. P. Matousek and M.D. Morris, editors, Springer-Verlag; (2010)

19. R. Stadelmann, M. Lugovy, N. Orlovskaya, P. Mchaffey, M. Radovic, V. M. Sglavo, S. Grasso and M. J. Reece, "Mechanical Properties and Residual Stresses in ZrB_2 – SiC Spark Plasma Sintered Ceramic Composites", *J European Ceramic Soc.*, **36** [7] 1527-1537 (2016)

20. W. D. Kingery, "Note on Thermal Expansion and Microstresses in Two-Phase Compositions". *J American Ceramioc Soc.*, **40** [10] 351-352 (1957)

21. P. S. Turner, "Thermal-Expansion Stress in Reinforced Plastics". *Journal of Research of the National Bureau of Standards*, **37**, 230-250 (1946)

22. Z. Li and R. C. Bradt, "Thermal Expansion and Thermal Expansion Anisotropy of SiC Polytypes". *J American Ceramic Soc.*, **70**, 445-448 (1987)

23. R. Hull, *Properties of Crystalline Silicon*. London: INSPEC; (1999).

24. J. D. Schall, G. Gao, J. A. Harrison, "Elastic Constraints of Silicon Materials Calculated as a function of Temperature using a Parameterization of the Second-Generation Reactive Empirical Bond-Order Potential". *Physical Review B.,* **77** [11] 115-209 (2008)

Author Manuscript

This article is protected by copyright. All rights reserved

25. R. G. Munro, "NIST Materials Properties Databases for Advanced Ceramics" *Phys. Chem. Ref. Data.*, **5**, 1195-1203 (1997)

Captions

Figure 1. Light grey is unreacted free silicon and dark grey is SiC. a is an image of SC-2 RBSiC received from Coors Tek with 24 vol% unreacted free silicon. b is an image of KX01 with 42 vol% unreacted free silicon.

Figure 2. Sum of the integrated intensities of the silicon (111), (220),and (311) powder diffraction peaks divided by the sum of the integrated intensities of the silicon and SiC (101), (102),(103),(104) and (110) diffraction peaks versus the weight percent of powder Si added to the KX01 RBSiC materials.

Figure 3. The images in part A at the top indicate the positions in the sample where each individual spectrum came from. The black circles indicate the location of the 20 μm diameter Raman probe for four locations in a high-Si sample. Part B is the Raman spectrum for the four locations shown in part A for the high-Si RBSiC. Part C provides detailed Raman spectra of the 520 cm^{-1} peak from silicon with the spectra from the four locations. The solid vertical line indicates the location of the unstressed peak position for silicon (520 cm^{-1}). In part D, we show the detailed Raman spectra of the 797 cm^{-1} peak from SiC with spectra from the four locations. The solid vertical line indicates the location of the unstressed peak position for SiC (797 cm^{-1}).

Figure 4. The images in part A indicate the positions in the sample where each individual spectrum came from. The black circles indicate the location of the 20 μm diameter Raman probe for four locations in a low-Si sample. Part B is the Raman spectrum for the four locations shown in part A for the low-Si grade RBSiC received from Coors Tek. Part C provides detailed Raman spectra of the 520 cm^{-1} peak from silicon with the spectra from the four locations. The solid vertical line indicates the location of the unstressed peak position for silicon (520 cm^{-1}). In part D, we show the detailed Raman spectra of the 797 cm^{-1} peak from SiC with spectra from the four locations. The solid vertical line indicates the location of the unstressed peak position for SiC (797 cm^{-1}).

This article is protected by copyright. All rights reserved

Author Manuscript

Table I. Results of peak fitting the Raman spectrum of the positions specified in Figures 3 and 4

Material	Position	Silicon Peak Position [cm^{-1}]	Compressive Microstress in Silicon [GPa]	SiC Peak Position [cm^{-1}]	Tensile Microstress in SiC [GPa]
High-Silicon	a	522.92 ± .04	1.74 ± .03	788.62 ± .13	2.37 ± .04
	b	522.88 ± .05	1.77 ± .03	788.81 ± .09	2.32 ± .02
	c	522.97 ± .05	1.77 ± .03	789.26 ± .33	2.19 ± .09
	d	523.16 ± .04	1.88 ± .03	789.47 ± .12	2.13 ± .03
Low-Silicon	a	522.97 ± .07	1.77 ± .04	789.47 ± .38	2.13 ± .11
	b	523.50 ± .06	2.08 ± .04	789.42 ± .27	2.15 ± .08
	c	523.20 ± .09	1.90 ± .05	789.60 ± .32	2.10 ± .09
	d	523.09 ± .11	1.84 ± .06	789.79 ± .39	2.43 ± .11

Table II. Results for Silicon Microstress state from Raman Spectroscopy in RBSiC

Material	Sample Name	Compressive Residual Microstress in Silicon [GPa]	Tensile Residual Microstress in SiC [GPa]
Low-Silicon	CT-HT-01	1.85 ± .25	2.16 ± .39
	CT-HT-02	1.99 ± .17	2.15 ± .38
	CT-HT-03	1.90 ± .16	2.13 ± .35
	CT-HT-04	1.94 ± .20	2.16 ± .41

This article is protected by copyright. All rights reserved

Author Manuscript

High-Silicon	KX01-6D-01	1.68 ± .23	2.33 ± .36
	KX01-6D-02	1.77 ± .33	2.27 ± .32
	KX01-6D-03	1.78 ± .22	2.28 ± .36
	KX01-6D-04	1.79 ± .21	2.22 ± .38

Table III. Relevant values used in Kingery-Turner equations

Material	Phase	K [GPa]	V [%]
Low-Silicon	Silicon	100	24
	SiC	200	76
High-Silicon	Silicon	100	42
	SiC	200	58

Table IV. Adapted values and measured values for stresses in SiC and silicon

Material	Average Measured Compressive Microstress in Silicon [GPa]	Compressive Microstress in Silicon from Thermoelastic Kingery-Turner model [GPa]	Average Measured Tensile Microstress in SiC [GPa]	Tensile Microstress in SiC from Thermoelastic Kingery-Turner model [GPa]
Low-Silicon	1.92 ± .11	0.10	2.12 ± .22	0.031
High-Silicon	1.76 ± .15	0.085	2.28 ± .10	0.061

Table V. Predicted values and measured values for stresses in SiC and silicon

This article is protected by copyright. All rights reserved

Author Manuscript

Material	Average Measured Compressive Microstress in Silicon [GPa]	Compressive Microstress in Silicon from Crystallization Strain - Modified Kingery-Turner model [GPa]	Average Measured Tensile Microstress in SiC [GPa]	Tensile Microstress in SiC from Crystallization Strain - Modified Kingery-Turner model [GPa]
Low-Silicon	1.92 ± .11	3.12	2.12 ± .22	0.99
High-Silicon	1.76 ± .15	2.66	2.28 ± .10	1.92

Author Manuscript

This article is protected by copyright. All rights reserved

Author Manuscript

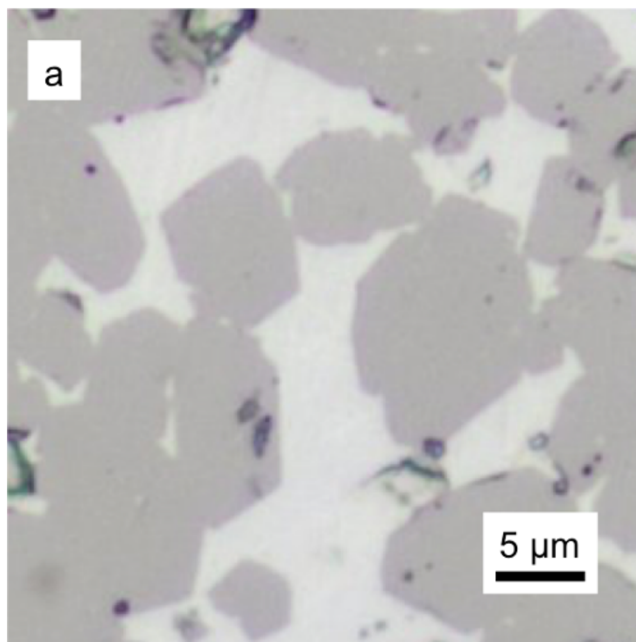

jace_14398_f1a.tif

This article is protected by copyright. All rights reserved

Author Manuscript

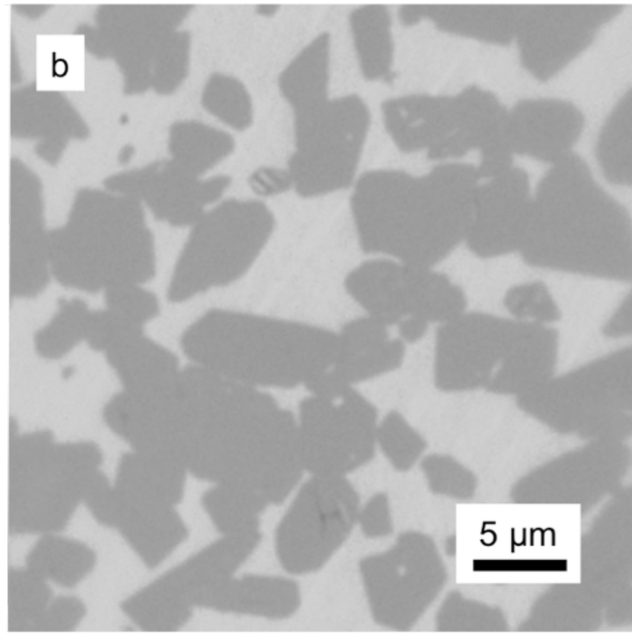

jace_14398_f1b.tif

This article is protected by copyright. All rights reserved

Author Manuscript

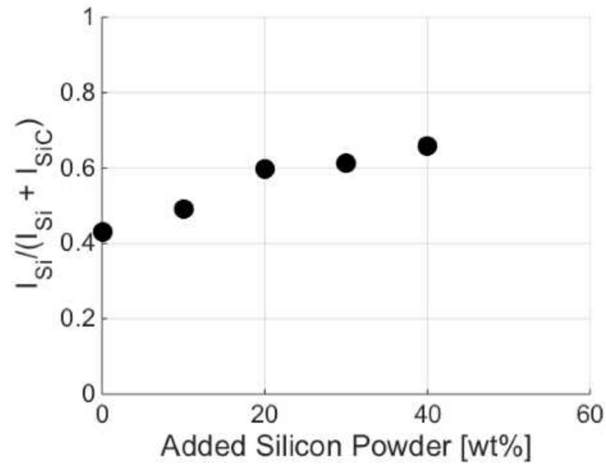

jace_14398_f2.tif

This article is protected by copyright. All rights reserved

Author Manuscript

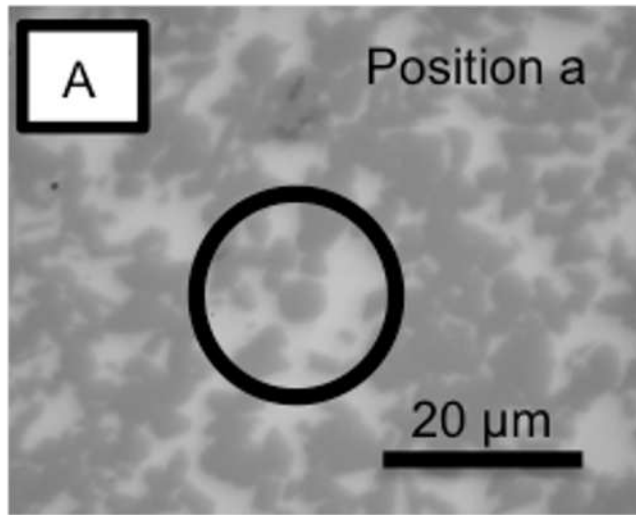

jace_14398_f3a.tif

This article is protected by copyright. All rights reserved

Author Manuscript

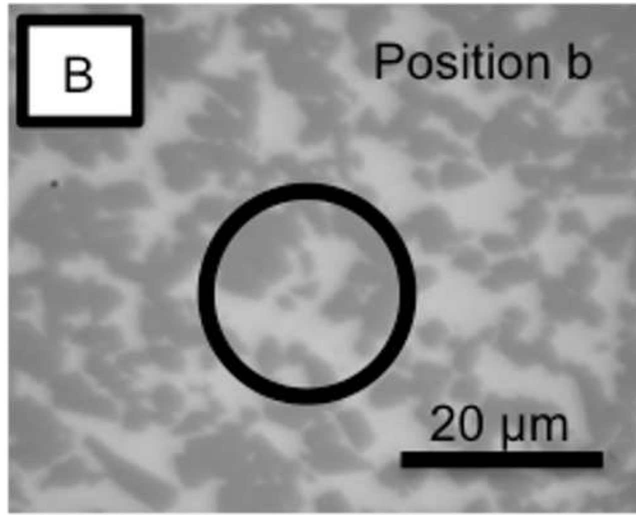

jace_14398_f3b.tif

This article is protected by copyright. All rights reserved

Author Manuscript

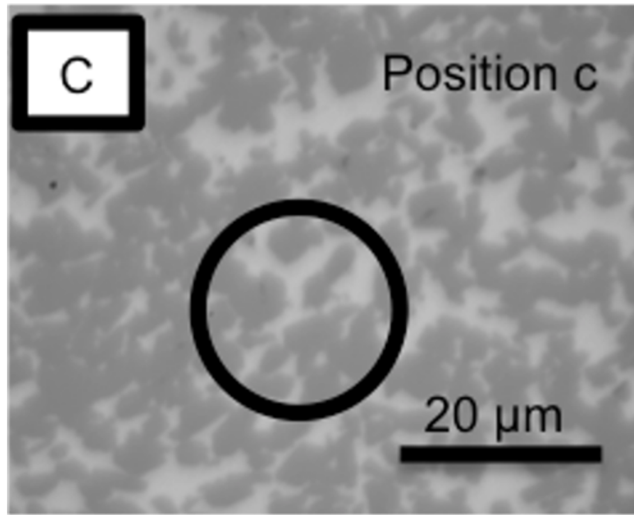

jace_14398_f3c.tif

This article is protected by copyright. All rights reserved

Author Manuscript

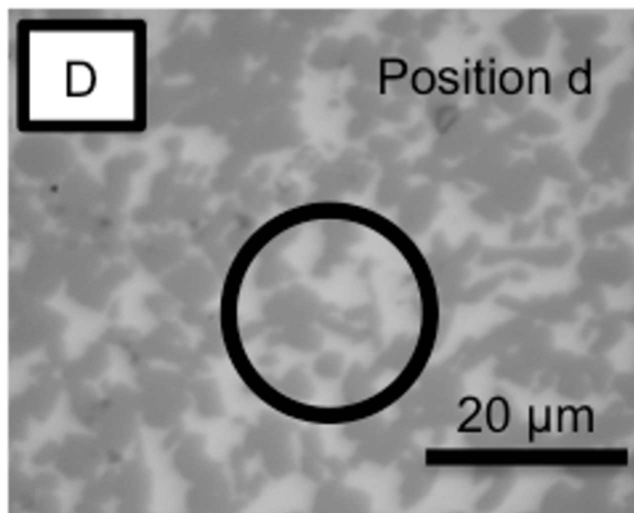

jace_14398_f3d.tif

This article is protected by copyright. All rights reserved

Author Manuscript

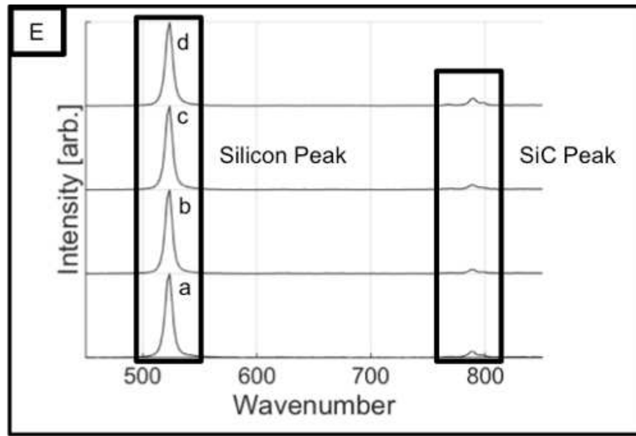

jace_14398_f3e.tif

This article is protected by copyright. All rights reserved

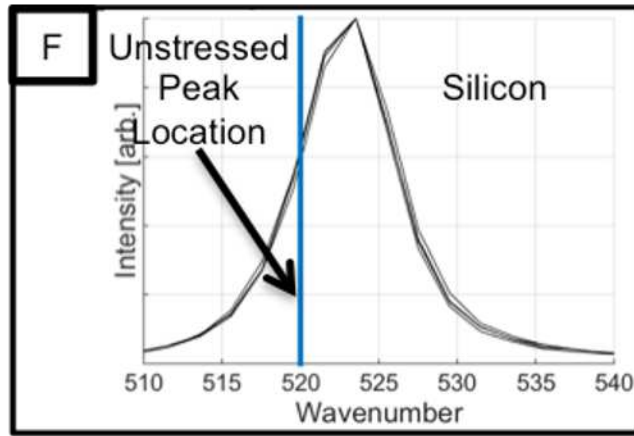

jace_14398_f3f.tif

Author Manuscript

This article is protected by copyright. All rights reserved

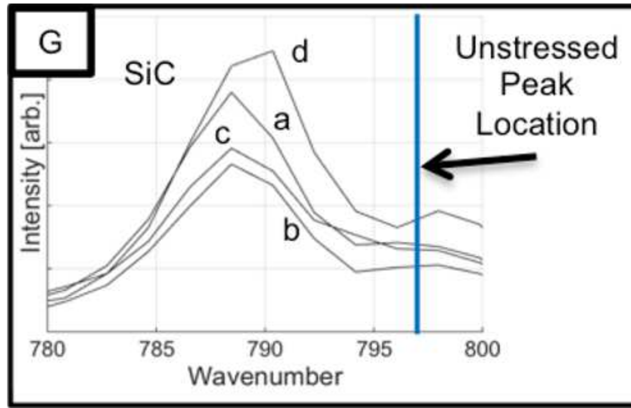

jace_14398_f3g.tif

Author Manuscript

This article is protected by copyright. All rights reserved

Author Manuscript

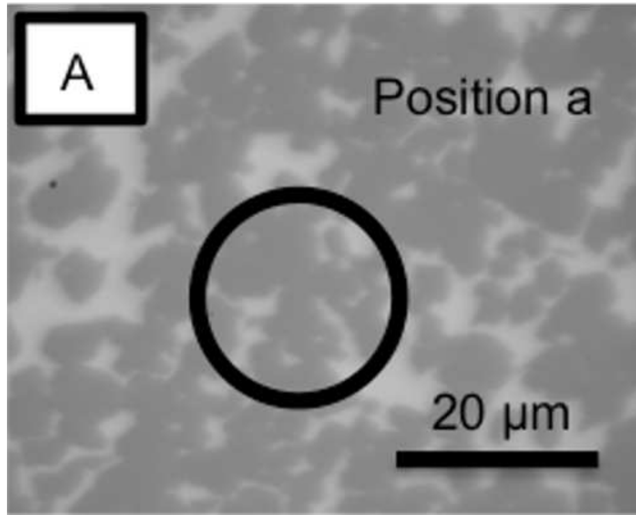

jace_14398_f4a.tif

This article is protected by copyright. All rights reserved

Author Manuscript

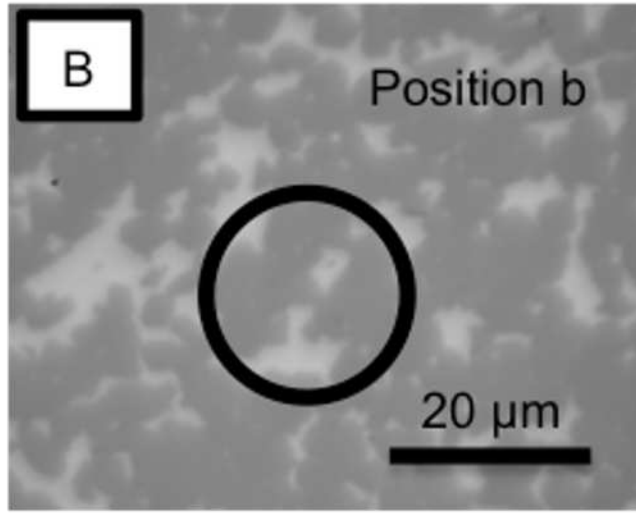

jace_14398_f4b.tif

This article is protected by copyright. All rights reserved

Author Manuscript

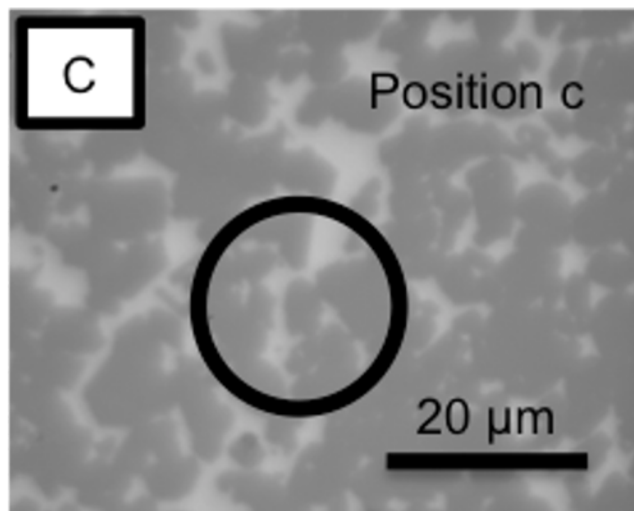

jace_14398_f4c.tif

This article is protected by copyright. All rights reserved

Author Manuscript

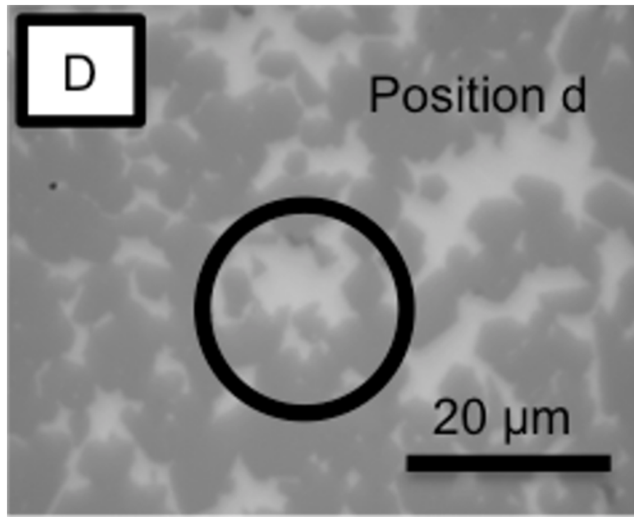

jace_14398_f4d.tif

This article is protected by copyright. All rights reserved

Author Manuscript

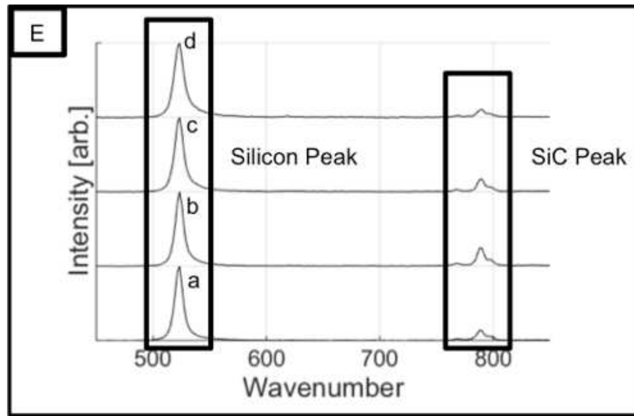

jace_14398_f4e.tif

This article is protected by copyright. All rights reserved

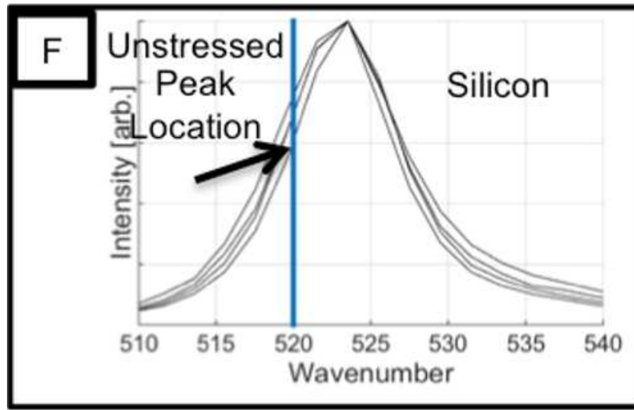

jace_14398_f4f.tif

Author Manuscript

This article is protected by copyright. All rights reserved

Author Manuscript

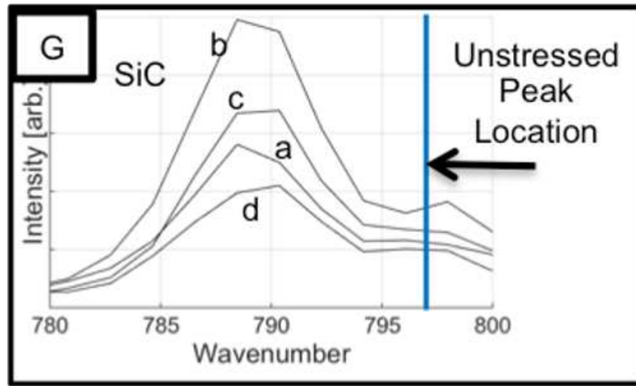

jace_14398_f4g.tif

This article is protected by copyright. All rights reserved